Institution of MECHANICAL ENGINEERS

1 Birdcage Walk
Westminster
London SW1H 9JJ

t. +44 (0)20 7222 7899
f. +44 (0)20 7222 4577

enquiries@imeche.org
www.imeche.org

One-dimensional simulation of the pressurized motoring method: friction, blow-by, temperatures and heat transfer analysis

C. Caruana[a], M. Farrugia[a], G. Sammut[b], E. Pipitone[c]

[a] Mechanical Engineering, University of Malta, Malta

[b] Jaguar & Land Rover Ltd., United Kingdom

[c] Department of Engineering, University of Palermo, Italy

ABSTRACT

Mechanical friction in internal combustion engines is nowadays largely optimized as a result of long years of research in this field. The ever increasing demand for better performance and less emissions however still puts mechanical friction as one of the areas in which further improvements can be done. This requirement calls for more accurate one-dimensional simulation models, along with reliable and robust experimental data to support such models. At University of Malta, a Pressurized Motoring test rig was developed and reported in SAE paper 2018-01-0121. Such method has proved to be relatively accurate in determining the mechanical friction of an internal combustion engine. As compared to the conventional Indicating technique, Morse test and Breakdown test, the Pressurized Motoring method offers the robustness that the uncertainty in the FMEP, as a result of error propagation is kept low. Furthermore, amendments to the traditional Pressurized Motoring technique were also done and presented in SAE paper 2019-01-0930, where Argon was used in place of Air to raise the bulk in-cylinder peak temperature to a value similar to what is found in a fired engine. In this proposal for publication, the authors now discuss a simple one-dimensional simulation model whose results are compared with those obtained and reported in SAE paper 2019-24-0141. Such work is aimed to test traditional friction and heat transfer models in one-dimensional software whilst identifying potential optimizations that can be done to the developed Pressurized Motoring test rig for its data to be more appealing to the one-dimensional researcher.

LIST OF SYMBOLS

$\dot{m}$	Mass flow rate
A_{valve}	Valve Area
N_v	Number of Valves
ρ	Fluid Density
ΔP	Difference in pressure
P_{up}	Upstream Pressure
P_{atm}	Atmospheric Pressure
γ	Ratio of Specific Heats
R	Specific Gas Constant
T_{up}	Upstream Temperature
C_f	Flow Coefficient
C_d	Discharge Coefficient
D	Diameter
L	Lift
$\dot{V}$	Volumetric Flow Rate
P	Downstream Pressure
P_{max}	Maximum In-Cylinder Pressure
Q	Heat Energy
V	Volume
U	Internal Energy
m	Mass
$p_{crankcase}$	Crankcase Pressure
$A_{orifice}$	Orifice Area

INTRODUCTION

Mechanical friction and heat transfer measurements are known to be fundamental to engine research and development, especially in an era when the internal combustion engine is facing stringent requirements to be met. At University of Malta, a Pressurized Motoring setup was built and tested (1) in which the exhausted gas of the motored engine is rerouted back to the intake side via a shunt pipe. This setup proved to allow for robust friction data to be obtained, due to mitigation of error propagation. Apart from the shunt pipe, which is relatively simple to realize, such method also proved to require no extra apparatus than what is usually available in a conventional engine test cell. The use of the shunt pipe minimizes greatly the quantity of gas required to be supplied for achieving peak in-cylinder pressures similar to that in fired engines, in fact a conventional shop floor compressor was found to be more than adequate (1). In a recent research (2), the engine was also operated on Argon, instead of Air, in order to address one of the main limitations of any motoring testing method, i.e. the low in-cylinder temperatures. The main aim of this complete research project was to provide the one-dimensional researcher with reliable experimental data to compare against traditional friction and heat transfer models as used in one-dimensional simulation software. This publication presents a simple one-dimensional model of the pressurized motoring setup used in (1) (2) (3) which was calibrated against the experimental results presented in (3).

Engine Geometry

The specifications for the engine in the one-dimensional model were made to match those of the engine used in (1) (2) (3) and presented in Table 1. The engine is an under-square with the pistons having three rings. The piston bowl shape has a relatively deep dish with a protruding sphere as shown in Figure 1. The pistons are also jet-cooled. The cylinder head chamber is flat with two valves per cylinder. The log-style intake manifold is shown in Figure 2 while the exhaust manifold is shown in Figure 3. The OEM exhaust manifold has an EGR port which in the pressurized motoring configuration was instead used for regulated gas supply. The intake manifold is made of cast Aluminum, whereas the exhaust manifold is made of cast Iron. The intake port in the cylinder head has a curved nature to impose swirl to the gas induced. The exhaust port has only an approximate $90°$ short bend. All intake and exhaust ports are identical.

Figure 1: OEM Piston

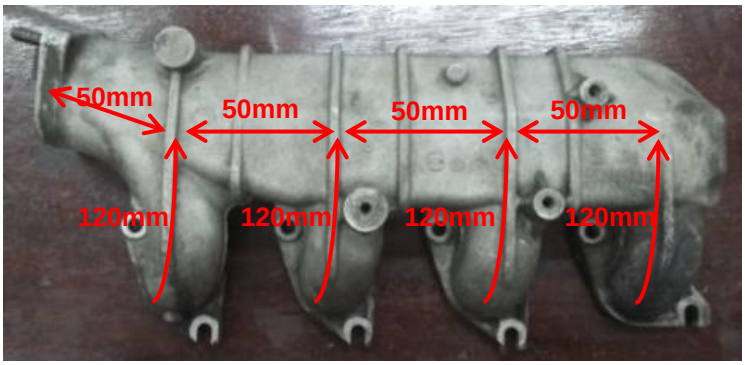

Intake Manifold:
Runner Diameter: 35mm
Plenum Cross-Sectional Area: 70mm x 50mm
Intake Manifold Entry Diameter: 40mm

Cylinder Head Intake Side:
Port Length: 120mm
Port Diameter: 35mm to 30mm

Figure 2: OEM Intake Manifold

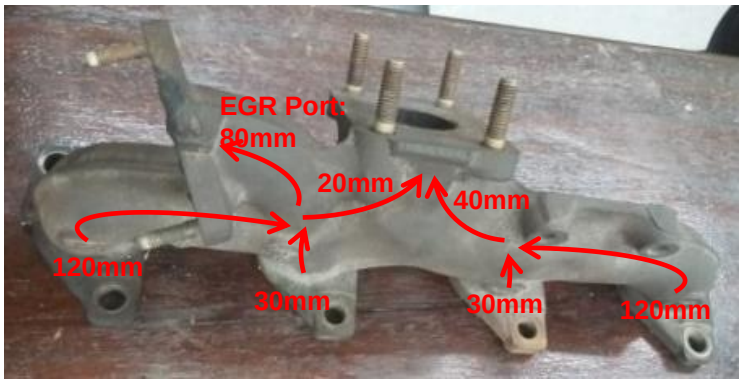

Exhaust Manifold:
Runner Diameter: 30mm
Exhaust Manifold Exit Diameter: 45mm
EGR Diameter: 25mm
EGR Length: 80mm

Cylinder Head Exhaust Side:
Port Length: 95mm
Port Diameter: 30mm

Figure 3: OEM Exhaust Manifold

Table 1: Engine Specifications

Make and Model	Peugeot 306 2.0HDi
Year of Manufacture	2000
Number of Strokes	4
Number of Cylinders	4
Valvetrain	8 Valve, OHC

Compression Ratio	18:1
Engine Displacement [cc]	1997
Bore [mm]	85
Stroke [mm]	88
Connecting Rod Length [mm]	145
Intake Valve Diameter [mm]	35.6
Exhaust Valve Diameter [mm]	33.8
Intake Valve Opens (1mm lift)	170 CAD BBDC intake
Intake Valve Closes (1mm lift)	20 CAD ATDC compression
Exhaust Valve Opens (1mm lift)	45 CAD BBDC expansion
Exhaust Valve Closes (1mm lift)	10 CAD BTDC exhaust
Intake Max. Valve Lift [mm]	9.6
Exhaust Max. Valve Lift [mm]	9.7

BUILDING THE ONE-DIMENSIONAL MODEL

In this research, Ricardo WAVE was used as the one-dimensional simulation software. The one-dimensional model discussed was initially developed by Camilleri (4) some years back when the engine was still used in the fired mode. During that time, the engine was coupled to a water-brake dynamometer in the aim of developing a programmable engine management for common rail diesel engines (5). The model was now modified to suit the new setup configuration of the Pressurized Motoring. The canvas for the one-dimensional model is shown in Figure 4.

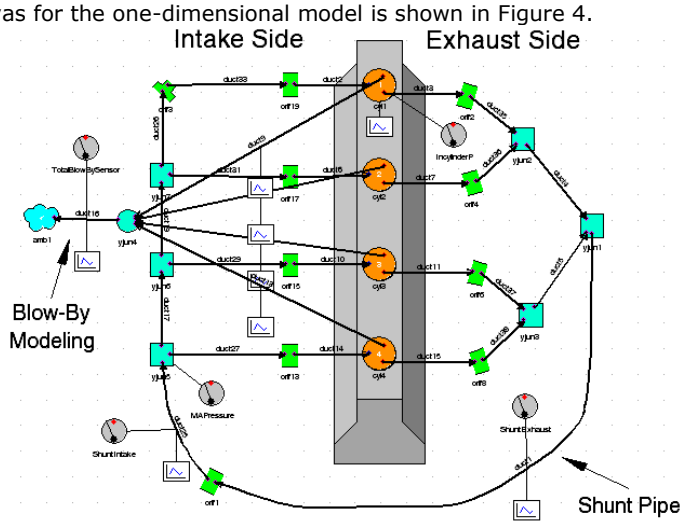

Figure 4: One-Dimensional Model Canvas

In building the one-dimensional model, all relevant lengths and diameters for the ports, manifolds and shunt pipe were entered as measured on the real designs. The ports were assigned a discharge coefficient of unity. Their bend angle, as well as friction coefficient were switched off, since their inefficiency was accounted for in the valve flow coefficients, which in this study were experimentally obtained. Valve lift profiles were also measured and made available by Camilleri (4). Experimental data for the manifold temperatures was not available; however experimental coolant temperatures were measured and used in the model. The wall temperature for the manifolds was set to around 15°C lower than that of the coolant for the particular setpoint considered.

The sub-models used in this one-dimensional model were primarily two; that for heat transfer and that for mechanical friction. Ricardo WAVE presents three alternatives to heat transfer estimation; Annand's model (6), Woschni's model (7) and Colburn's model. Apart from these, WAVE allows for the IRIS and a user-defined heat transfer model. In this study, the model by Annand and Woschni were used separately as discussed later in the paper.

The only friction model offered by Ricardo WAVE is that based on the Chen-Flynn correlation (8). Such model consists of four terms representing the friction contribution due to engine speed, engine load, windage and accessories. The results from this correlation are discussed in the results section.

Additional sub-models like the conduction model and the thermocouple model were also considered and used, but preferred to turn them off for the final version of the model as their results were questionable.

Parameters like the thermodynamic loss angle are known to be sensitive to blow-by flow (9), even though its effect is minimal compared to heat transfer. Since experimental data for blow-by flow was available, a blow-by model was devised as suggested by WAVE knowledge centre (8). The model consists of a third valve on each cylinder of the orifice type. Each of these valves were connected to a large volume, representing the crankcase and exhausted to atmosphere, represented by an 'Ambient' element. The diameter of the orifice valve was varied until the blow-by flow on each setpoint matched that obtained from the experimental sessions (1).

Cylinder Head Flow Testing

In support of developing the WAVE model, an experimental test session was performed on an in-house developed flow-bench in the aim of determining the valves' discharge and flow coefficients. The cylinder head used in this testing session was of the same make and model of the 2.0HDi engine used on the Pressurized Motoring Setup and the one-dimensional model. All tests carried out on the flow-bench were done at 28" of water (i.e. 7kPa) below atmospheric conditions for pull through configuration (port to cylinder), and above atmospheric conditions for blow through configuration (cylinder to port). Temporary bellmouth using modeling clay were manually formed at entrance as is common practice in flow bench testing.

When set up on the flow-bench, the cylinder head was in the condition as dismantled from the running engine, i.e. not cleaned. It was discovered that since the particular engine has an EGR system, the intake valves contained heavy soot deposits on their back end as seen in Figure 5. The cylinder head was flow tested in this condition and the flow coefficients were determined in this state. Later, the valves were thoroughly cleaned and flow tested again. Figure 6 shows the mass flow comparison between two clean intake valves and the same valves before cleaning. It is clearly visible that when clean, the two valves have relatively similar flow behaviors, whereas before cleaning, the flow was marginally lower for valve 3 and considerably lower for valve 2, dependent on the amount and shape of the deposited soot. The exhaust valves were also checked for soot deposition, but it was noted that the amount of soot present was not abnormal to that usually found on exhaust valves. All exhaust valves were cleaned prior flow testing.

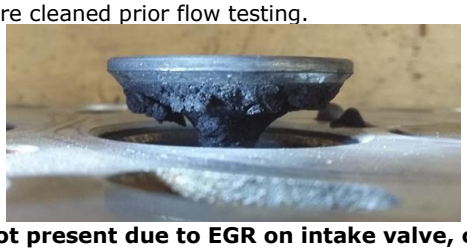

Figure 5: Soot present due to EGR on intake valve, cylinder two.

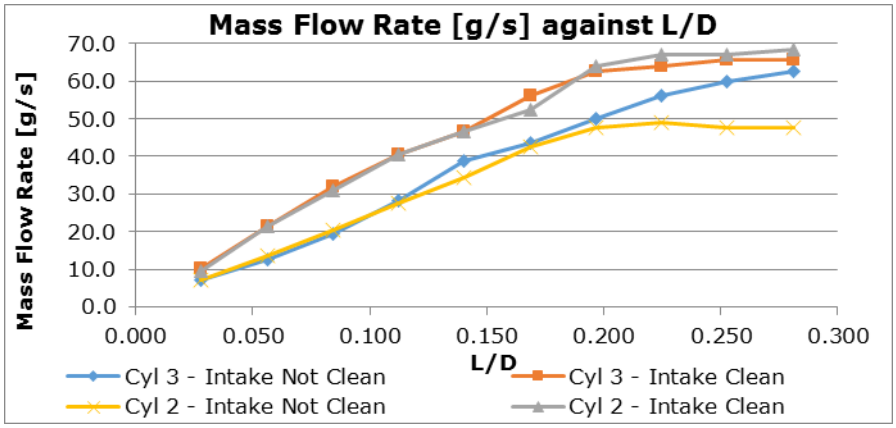

Figure 6: The Graph of Mass Flow Rate [g/s] against L/D, showing difference between clean and sooted intake valves

The second aim of this flow testing session was to determine the restriction that both the intake and exhaust manifolds had on the mass flow. Figure 7 shows that the intake manifold was not a major restrictor at low lifts, but did restrict the flow at higher lift values. The exhaust manifold on the other hand seems to have aided the flow through the exhaust valve at lower lifts but restricted it at higher lifts.

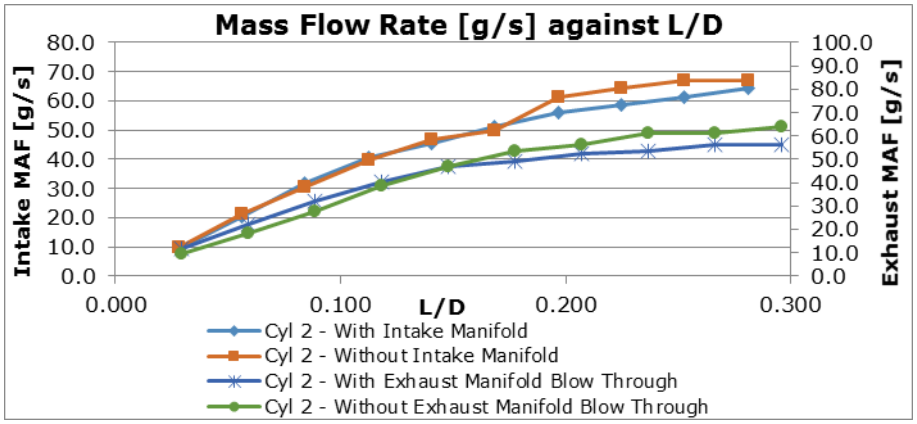

Figure 7: The graph of mass flow [g/s] against L/D showing effect of manifolds

The exhaust valves were tested with two flow configurations; 'blow through' (i.e. from the cylinder to the port) and 'pull through' (i.e. from the port into the cylinder). The two results were compared and shown in Figure 8. In usual flow bench practice the exhaust valve is tested with a blow through setup to mimic better the actual flow direction in the engine. To follow such practice, in the one-dimension simulation software, the flow coefficient obtained from the blow through test data was used for the exhaust.

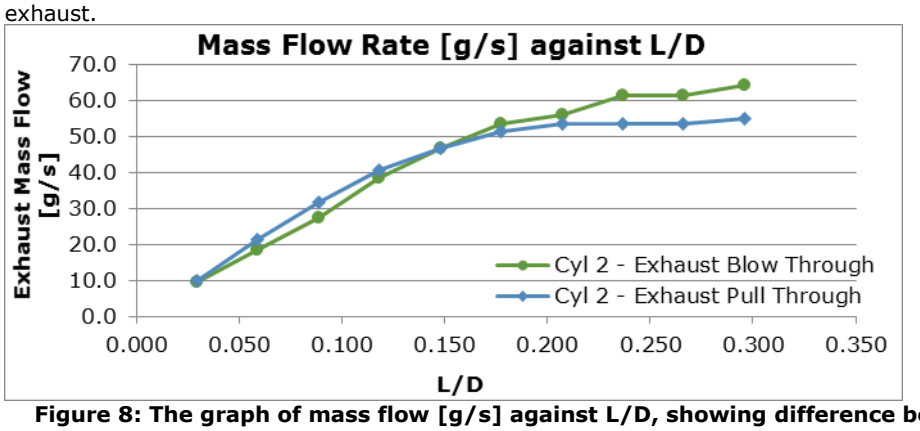

Figure 8: The graph of mass flow [g/s] against L/D, showing difference between blow through and pull through.

The 2.0HDi cylinder head ports are known to be relatively identical between cylinders. On the other hand however, the OEM exhaust manifold of the 2.0HDi is known to be unsymmetrical with respect to the manifold outlet. Due to this, it was deemed necessary to flow test each port with the manifold attached to determine the flow characteristic of each runner. Figure 9 shows that the second exhaust runner, which coincidently is the shortest and straightest of the four seems to flow in excess of 7g/s more than the least flowing runner, i.e. that of cylinder 3.

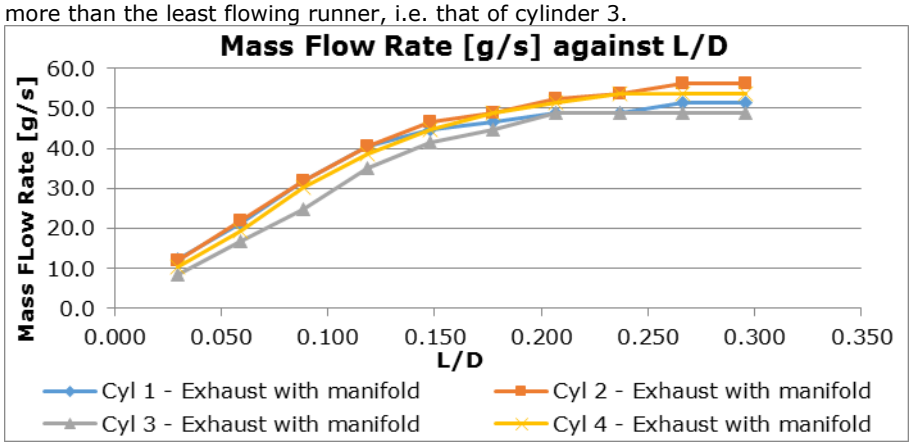

Figure 9: The graph of mass flow rate [g/s] against L/D showing difference between each exhaust runner.

Verification of Flow Coefficients through 1D simulation

In obtaining the flow coefficients from the mass flow experimental data, three equations were used and reported below in 1, 2 and 3. Equation 1, derived from Bernoulli's equation assumes an incompressible flow. Both equation 2 from Heywood (10) and equation 3 from Ricardo Knowledge Centre (8) assume a compressible flow. Equation 4 gives the discharge coefficient and is given by Ricardo Knowledge Centre (8). Both the coefficient of flow and coefficient of discharge can be inputted in WAVE. During runtime, the software will automatically detect whether the information given is C_f or C_d, based on the first point inputted in the array.

$$C_f = \frac{\dot{m}}{A_{valve} N_v \sqrt{2 \rho \Delta P}} \quad \ldots(1)$$

$$C_f = \frac{\dot{m}}{A_{valve} N_v P_{up} \frac{1}{\sqrt{R T_{up}}} \left(\frac{P_{atm} - \Delta P}{P_{up}}\right)^{\frac{1}{\gamma}} \left(\frac{2\gamma}{\gamma - 1}\right)^{\frac{1}{2}} \left[1 - \left(\frac{P_{atm} - \Delta P}{P_{up}}\right)^{\frac{\gamma - 1}{\gamma}}\right]^{\frac{1}{2}}} \quad \ldots(2)$$

$$C_f = \frac{4 A_{eff}}{\pi D^2} \quad \ldots(3)$$

$$C_d = \frac{A_{eff}}{\pi D L} \quad \ldots(4)$$

Where

$$A_{eff} = \frac{\dot{V}}{\sqrt{2 \left(\frac{\gamma}{\gamma - 1}\right) R T_{up} \left[1 - \left(\frac{P}{P_{up}}\right)^{\frac{\gamma - 1}{\gamma}}\right]}} \quad \ldots(5)$$

To verify the flow coefficient calculation using equation 3, a steady-state model was built in Ricardo WAVE, using an orifice valve with configurable flow coefficient as input (11). This simulated the poppet valve in the experimental flow-bench setup having different flow coefficients at different lifts. The bore-tube adaptor used and the cylinder head port were also modeled, but switching off their friction and discharge coefficient models for the reason mentioned in the previous section. In the one-dimensional steady-state simulation, the flow coefficients obtained from experimental testing and using equation 3 were input as individual cases for different lift values and the mass flow was obtained in return. From this relatively simple check it transpired that the mass flow obtained using 1D simulation was within 2% of that obtained experimentally, as shown in Figure 10. This demonstrates that the flow coefficients calculated were correctly obtained.

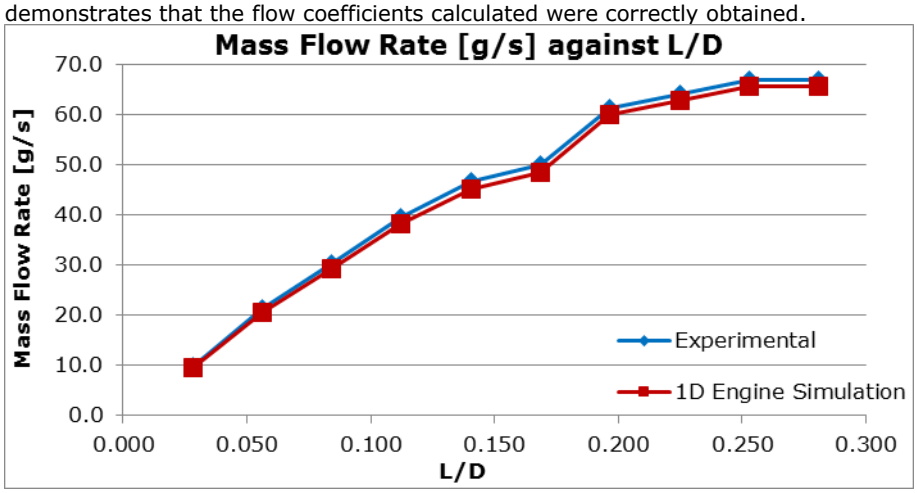

Figure 10: The graph of mass flow [g/s] against L/D comparing the experimental and simulated mass flow on intake valve.

RESULTS

In calibrating the pressurized motored one-dimensional model, the experimental data presented in (3) were used. The test matrix for such experimental data entailed engine speeds of 1400rpm, 2000rpm, 2500rpm and 3000rpm with a peak in-cylinder pressure of 84bar and gas compositions of gamma (c_p/c_v) 1.4, 1.5, 1.6 and 1.67, where 1.4 represents that of air and 1.67 represents that of pure argon. For the purpose of the one-dimensional modeling conducted in this study, all setpoints related to air were considered successfully, however the simulation software used did not support Argon and hence experimental data for gamma of 1.5, 1.6 and 1.67 could not be modeled.

To calibrate the one-dimensional model, the data as obtained from experiments were input as constants for the different setpoints tested. Such information includes the engine speed, manifold

absolute pressure, shunt pipe intake and exhaust temperatures, valve lifts, valve flow coefficients and the engine geometry. Results like Peak In-cylinder Pressure, Gross IMEP, PMEP, Net IMEP and FMEP were then obtained and compared to the experimental data presented in (3). With such strategy, similar results were obtained, however the discrepancy was still deemed too large for any qualitative deduction to be made.

One initial problem which was troublesome regarded the configuration with which the manifold pressure was being imposed in the one-dimensional simulation. Initially, the manifold pressurization was imposed by connecting an ambient element with forced pressure and temperature equal to the measured MAP and shunt pipe temperature respectively to the exhaust collector y-junction. Results showed that the manifold pressure being imposed on the one-dimensional simulation was resulting in very large deviations in the peak in-cylinder pressure. Such issue was traced down to the ambient condition which was imposing too strict of a boundary condition. To solve such problem the ambient element was removed, and instead the manifold pressure was imposed as an initial pressure condition to the shunt pipe (acting as an initial reservoir) with an additional extra pressure required to fill all ducts with the experimentally obtained MAP, whilst allowing also some flow as blow-by. The initial extra pressure in the shunt pipe was adjusted until the final condition in all manifolds matched that obtained from the experimental MAP sensor to within $\pm$0.001bar. Later on in this work, such process was automated by using a PID controller responsible of varying the area of an orifice which connected an ambient element to the y-junction of the exhaust collector. With such configuration, better control of the MAP was obtained, whilst still retaining the system detached from the forced ambient element through the controlled orifice.

To understand further the discrepancy between simulation and experimental results, the trapped mass at IVC, obtained on each setpoint from the simulation was compared to that calculated using the ideal gas law equation on the respective experimental data. The trapped mass at IVC was matched to be within 10%. The in-cylinder pressure curve against crank angle was then obtained from the one-dimensional model for each setpoint and plotted against the relevant $p - \theta$ curve from the corresponding experimental data. To be able to compare the two traces, the experimental pressure curve had to be pegged on the intake stroke to the trace obtained from the one-dimensional software. When pegging was attempted, it was seen that an acceptable match was evident between the wave nature of the simulation in-cylinder pressure intake stroke, and that obtained experimentally. Also, the simulation exhaust stroke in-cylinder pressure seemed to show well the recompression on the exhaust displacement phase, visible also in the experimental data. The phasing and magnitude of this recompression however were slightly different. To rectify the issue, an attempt was made to assign 0.3mm of valve lash to each of the intake and exhaust valves. On this amendment, the in-cylinder pressure curve on the intake and exhaust strokes obtained from the simulation matched even better in its wave nature to that obtained from the experimental data. This was noted on all the setpoints tested and hence pegging could be now done not just at one crank angle, but on the whole intake stroke. Figure 11 shows the intake stroke comparison between that obtained from the simulation and the experimental data for two of the setpoints. It should be noted that the simulation model gives the possibility of pegging the experimental data to the in-cylinder pressure generated. Randolph (12) in his publication mentions method 8 of pegging to the ideal gas law equation, but stated that such method does not take into consideration the heat and blow-by losses. However it can now be noted that such issue is catered for when pegging to the simulation in-cylinder pressure.

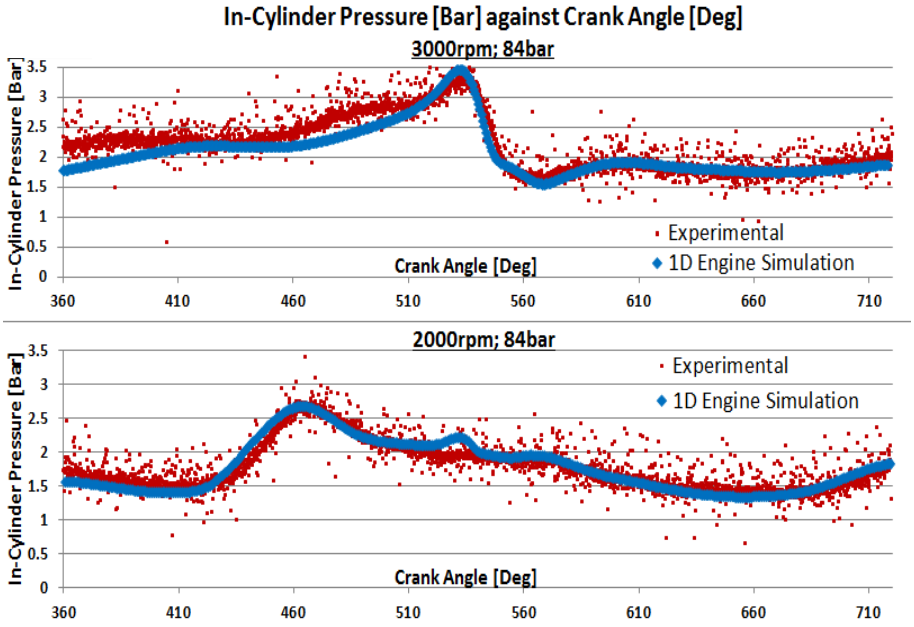

Figure 11: The graph of In-cylinder Pressure against Crank Angle on the intake and exhaust strokes for two different setpoints.

After pegging the traces on the whole intake strokes, the full 720° simulation in-cylinder pressure cycle was compared to that from the corresponding experimental data. It was shown that some discrepancy on the peak in-cylinder pressure was evident. The heat transfer multiplier on closed valve for the heat transfer correlation were tweaked in the hope of getting a match on the peak in-cylinder pressure, however it was seen that when the peak pressure was successfully matched, the in-cylinder pressure during the compression stroke for the simulation fell below that of the experimental pressure trace by a significant amount as seen in Figure 12a. A similar observation was noted on the expansion stroke. Such discrepancy on the compression and expansion strokes led to a 38% discrepancy in the gross IMEP on the setpoint of 3000rpm; 84bar between the simulation and experimental cases. To rectify this issue, the cylinder head, piston and liner temperatures were shifted to higher temperatures than the coolant temperature obtained experimentally by different amounts dependent on the engine speed setpoint, but not higher than the oil temperature of 80°C, as imposed experimentally. The higher the engine speed, the higher the temperature required due to a lesser time for heat to flow out of the system. Such amendment seemed to give a better all-around match between the simulation and experimental in-cylinder pressure traces as shown in Figure 12b. Consequently the gross IMEP showed a better match as well. Figure 13 shows the overall comparison between the simulation and experimental pressure traces on the same 3000rpm; 84bar. With such better comparison, the discrepancy in the Gross IMEP on the same setpoint of 3000rpm; 84bar was around 9%.

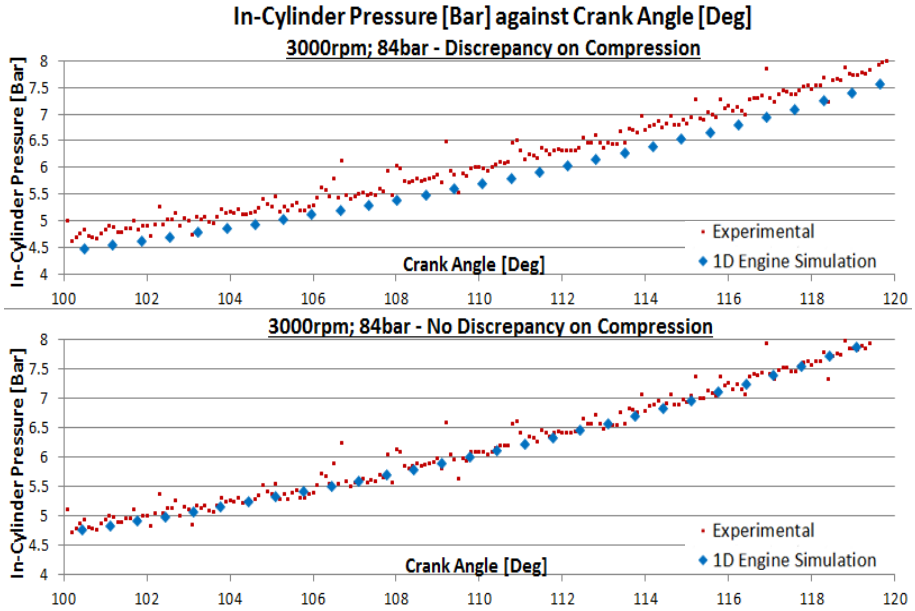

Figure 12: The graph of in-cylinder pressure against crank angle : a) Discrepancy on compression, b) No discrepancy on compression.

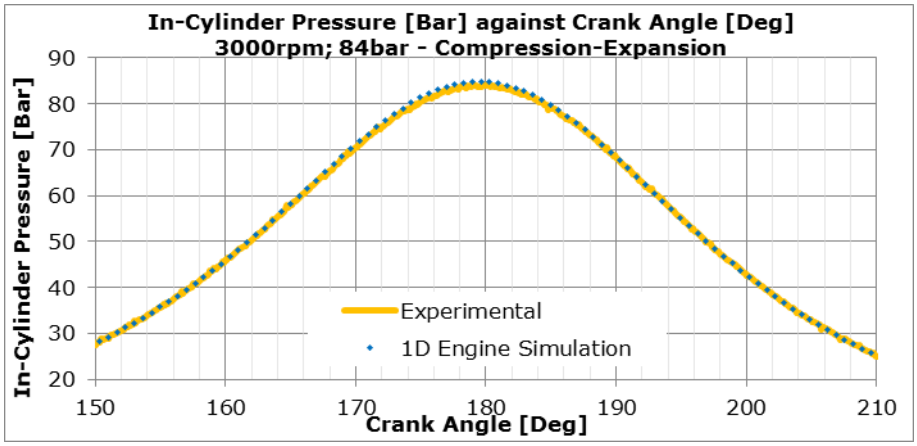

Figure 13: The graph of in-cylinder pressure against crank angle, showing comparison between experiment and simulation data on compression and expansion strokes.

Figure 14 to Figure 17 compare the results obtained from the experiments as reported in (3) to those obtained from the one-dimensional model using Annand's and Woschni's heat transfer model with intake scavenging (8). It can be seen that the IMEP gross matches relatively well between the experimental and simulation results, with a maximum deviation of around 7%. The BMEP also shows a very good match, however such quantity is not a true indicator of how well the simulation model compares to the experimental data. This is because deviations in IMEP gross, PMEP and FMEP having different signs might compensate for each other's deficiencies leading to a mistakenly interpreted good match on the BMEP.

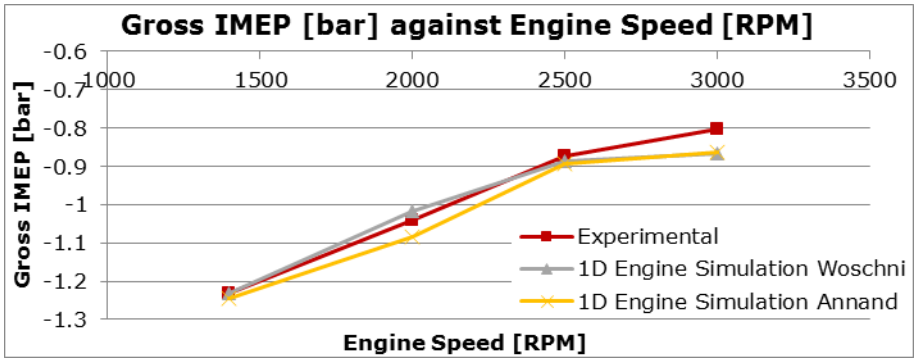

Figure 14: The gross IMEP graph comparing simulation and experimental results.

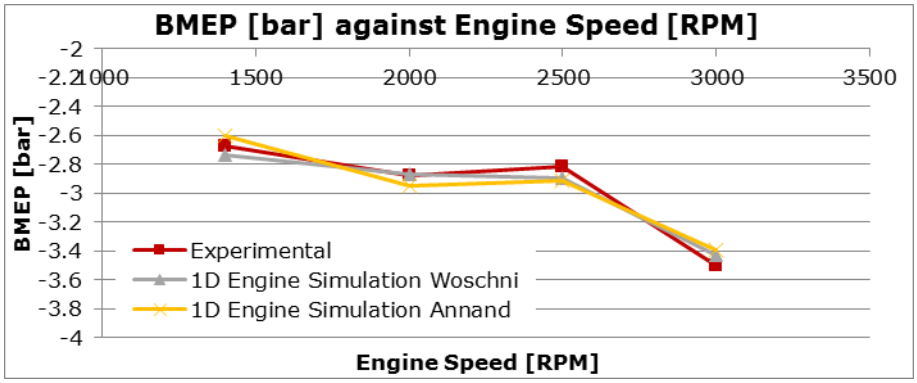

Figure 15: The BMEP graph comparing simulation and experimental results.

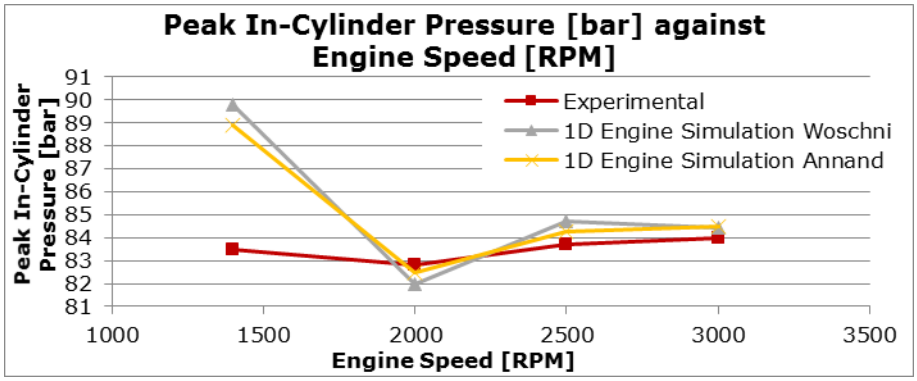

Figure 16: The peak in-cylinder pressure graph comparing simulation and experimental results.

The setpoint which seemed to show the largest deviation from that of the experimental data was the 1400rpm; 84bar. It was noted that this setpoint suffered from an error of 10% on the trapped mass at IVC, which consequently resulted in a higher peak in-cylinder pressure as seen in Figure 16.

Figure 17 shows the PMEP comparison between the simulated and experimentally obtained values. It can be seen that a very good match was obtained on all setpoints, with the 2500rpm and 3000rpm having the largest deviations. Such discrepancy on these setpoints was noted to have originated from a relatively different pressure wave on the exhaust stroke between the simulated and experimental data.

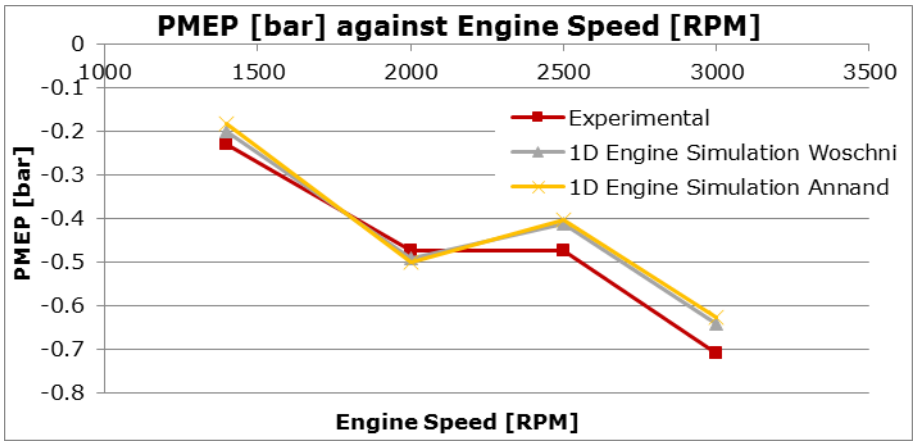

Figure 17: The PMEP graph comparing simulation and experimental results.

Friction Mean Effective Pressure

As mentioned earlier, the FMEP model used in this one-dimensional study was that by Chen and Flynn (8), given in equation 6. The Chen-Flynn coefficients were found through a regression analysis and documented in Table 2. The FMEP comparison between simulation and experimental data, given in Figure 18 shows an acceptable match with a maximum deviation of 10% and a total average deviation of around 4.5%. The coefficients in Table 2 were inputted in WAVE and used throughout this simulation study.

$$FMEP = A_{cf} + \frac{1}{n_{cyl}} \sum_{i=1}^{n_{cyl}} \left[B_{cf} P_{max_i} + C_{cf} \left(\frac{RPM\ x\ stroke}{2} \right) + Q_{cf} \left(\frac{RPM\ x\ stroke}{2} \right)^2 \right] \quad \ldots (6)$$

Table 2: Chen-Flynn Correlation Coefficients

ACF $[bar]$	0.5965
BCF	0.00421
CCF $[Pa.min/m]$	0.0000
QCF $[Pa.min^2/m^2]$	5.4572

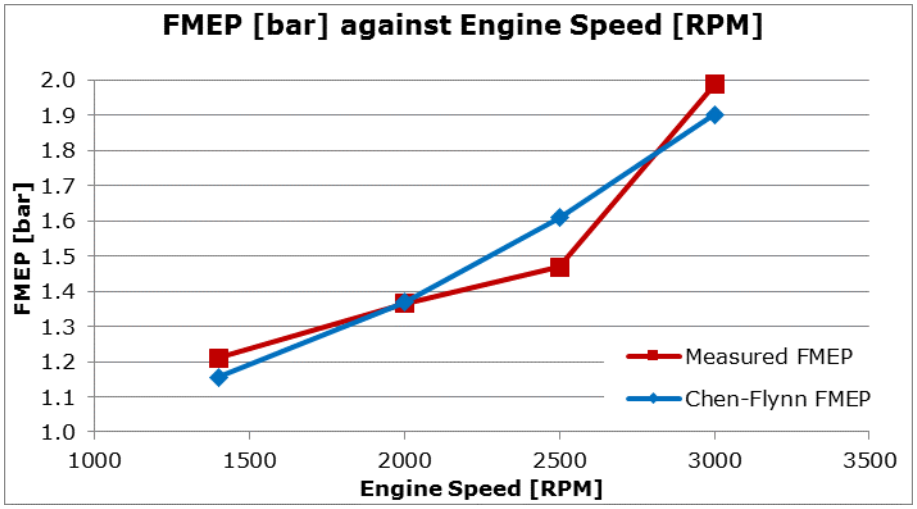

Figure 18: The FMEP graph comparing Chen-Flynn with experimental results.

Blow-By

As previously shown in Figure 4, a blow-by system was implemented in the one-dimensional model represented by a third orifice in each of the cylinders, as suggested by Ricardo WAVE knowledge centre (8). The orifice diameter was obtained by calibrating the model against the blow-by flow rate measured experimentally and published in (1). To obtain good agreement in blow-by flow rate on all setpoints between the experimental and simulation data, an orifice diameter of approximately 0.6mm was assigned. It was also noted that the peak in-cylinder pressure obtained through the simulation model had a large effect on the relatively small blow-by flow rate, meaning that a small deviation of the peak in-cylinder pressure from the setpoint of 84bar had a significant difference on the blow-by average value.

The blow-by flow rate was also computed on the experimental in-cylinder pressure data using equations 7 and 8 from (9). Figure 19 shows the comparison between the WAVE generated blow-by flow rate and that obtained from the experimental data, using equations 7 and 8.

For $\frac{p_{crankcase}}{p} > \left[\frac{p_{crankcase}}{p}\right]_{CR} \approx 0.53$

$$\dot{m} = A_{orifice}\sqrt{\frac{2\gamma}{\gamma-1}.m_a\frac{p}{V}.\left[\left(\frac{p_{crankcase}}{p}\right)^{\frac{2}{\gamma}} - \left(\frac{p_{crankcase}}{p}\right)^{\frac{\gamma+1}{\gamma}}\right]} \quad \ldots(7)$$

For $\frac{p_{crankcase}}{p} < \left[\frac{p_{crankcase}}{p}\right]_{CR} \approx 0.53$

$$\dot{m} = A_{orifice}\sqrt{\gamma.m_a\frac{p}{V}.\left(\frac{2}{\gamma+1}\right)^{\frac{\gamma+1}{\gamma-1}}} \quad \ldots(8)$$

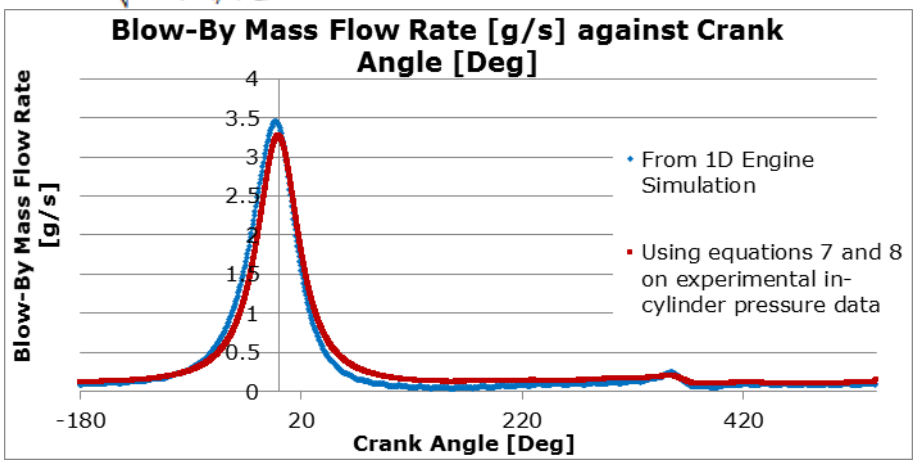

Figure 19: The graph of blow-by flow rate of cylinder 1 comparing that obtained from simulation and that obtained using eqns. 7 and 8 on experimental data - 3000rpm; 84bar

Figure 20 shows the transient blow-by flow rate for cylinder 1, the total blow-by flow rate as computed by a summation on the four cylinders, and the average total both for the summated and sensor-obtained total flow rate. It can be seen that the blow-by flow rate of each cylinder reflects the in-cylinder pressure trace, meaning that the blow-by flow-rate increases with the increasing in-cylinder pressure on compression stroke. At around 358° crank angle, a small increase in blow-by flow rate is evident, showing an increase in blow-by on the exhaust displacement phase. This is due to the recompression effect. The average values from the summated total and that obtained from the sensor were equal as shown in Figure 20.

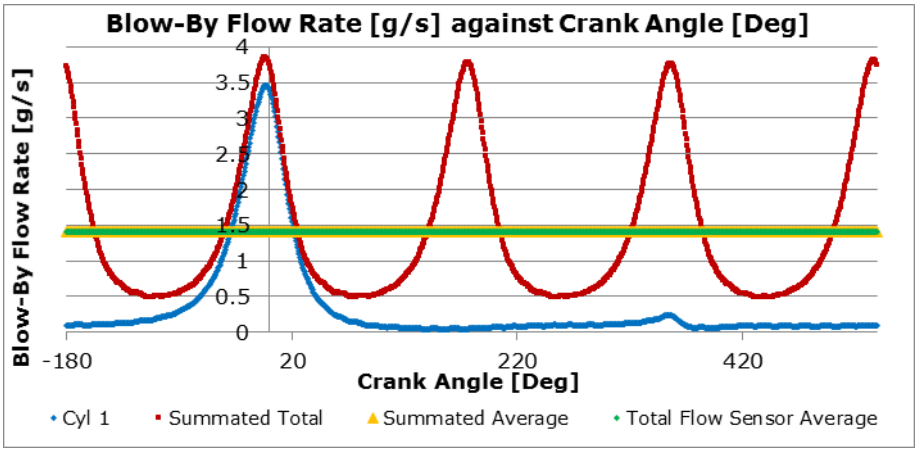

Figure 20: The crank-angle resolved blow-by flow rate graph obtained from simulation for cylinder 1, total, and total average on the setpoint of 3000rpm; 84bar.

In order to investigate the effect of blow-by on the simulation results, the model was re-run but with the blow-by system removed. It was noted that on the 3000rpm, 84bar the peak in-cylinder pressure increased from 84.5bar to 85.5bar. The IMEP gross magnitude decreased from 0.862bar to 0.777bar. Such variations are consistent with theory, since blow-by acts to reduce the peak in-cylinder pressure through leakage, while increases the magnitude of the overall losses. With no blow-by, the location of peak pressure is also expected to be closer to TDC. During this study it was noted that Ricardo WAVE obtains the location of peak pressure by finding the point of $\frac{dp}{d\theta} = 0$ on the polynomial fitted to the generated in-cylinder pressure curve. The crank angle resolution of the generated $p - \theta$ curve in the one-dimensional software was noted to vary with engine speed and was never better than 0.6DegCA. This therefore implies that the location of peak pressure as obtained from the one-dimensional software might be in disagreement compared to that obtained experimentally (which had a resolution of 0.1DegCA). At the 3000rpm; 84bar with the blow-by model activated, the one-dimensional model predicted a loss angle of -0.43DegCA, whereas with the blow-by model de-activated, the loss angle was estimated as -0.37DegCA. The experimental results gave a loss angle of -0.3DegCA on the same setpoint.

Heat Transfer

In this one-dimensional simulation, the heat transfer sub-models used were that by Annand (6) and Woschni (7). The multiplier on closed valve which was found to give a sensible compromise on the peak in-cylinder pressure was around 0.42 for Annand and 1.2 for Woschni on all the setpoints considered in this work. It should be noted that Annand's model was initially developed for a fired engine, and hence using this model for a pressurized motoring setup might be driving the model into unfavorable conditions. As said earlier, to have obtained an in-cylinder pressure trace which compares well to that obtained from experiments, a compromise had to be found between the heat transfer model, the cylinder head, piston and liner temperatures, compression ratio and trapped mass. It should be said that the compression ratio stated by the OEM for the engine tested is 18:1. This value was confirmed through a static compression ratio measurement using paraffin. It is however known that CR values do vary from that given in the engine manual (9). In fact, even if just the difference in thermal expansion is taken into consideration, for an engine with an aluminum cylinder block and steel connecting rod, when the connecting rod is at a temperature of 120℃ and the block is at 90℃, the static CR changes from 18:1 to 17.7:1. The engine used in this study does not have an aluminum cylinder block (cast iron block), but nonetheless the mechanical loading effect (due to in-cylinder pressure) on CR would still be present. The value of CR which was found to give the best compromise in this simulation study was that of 17.3:1.

Having used these variables, i.e. heat transfer, temperatures, CR and trapped mass to obtain reasonable pressure-theta curves, it was noted that the temperatures that had to be assigned to the cylinder head, piston and liner might have been different than the real temperature values, had they been measured. This means that the deficiency in the heat transfer models in predicting accurately the heat transfer in the pressurized motored engine might have had to be compensated for by fictitious temperatures in the cylinder head, piston and liner. To support such hypothesis, Figure 21 shows the in-cylinder temperature given by the simulation software and the heat transfer on the same cylinder as computed through Annand's and Woschni's model. According to experimental and analytical works by authors such as Lawton (13), Wendland (14) and Pinfold (15), the peak heat transfer in the cylinder should occur significantly earlier than the peak in-cylinder temperature because of pressure work in the boundary layer. Figure 21 however does not capture such effect, which therefore might consolidate the theory suggested earlier that the temperatures assigned to the

cylinder head, liner and piston might have been compensating for deficiencies in the heat transfer models.

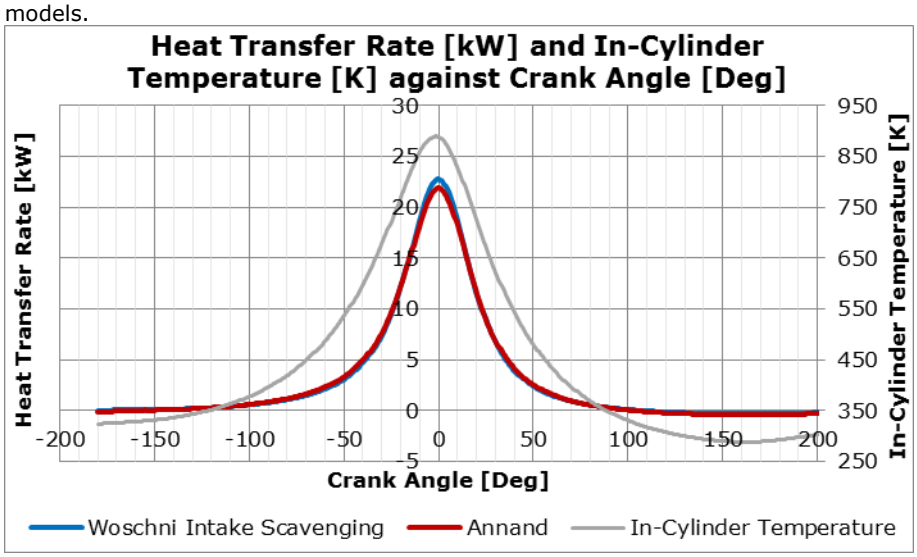

Figure 21: The graph of In-cylinder temperature and heat transfer rate obtained through Annand's and Woschni's correlation.

To further investigate such result, the Thermodynamics first law was considered on the system for the time in which valves are closed, i.e. compression and expansion strokes, as suggested by Heywood (16). Since no combustion is present in the setup being considered, the system resolves into equation 9, which further simplifies to equation 10, where mass flow due to blow-by is neglected. It should be said that since this equation does not account for blow-by, but the in-cylinder pressure on which such equation is used is reduced by the effect of blow-by, the heat transfer result obtained from equation 10 will be artificially greater to account for the effect of blow-by as heat lost. Equation 10 was used on the ensemble average experimental in-cylinder pressure data and plotted in Figure 22 for the 3000rpm; 84bar. It can be noted that due to small serrations in the in-cylinder pressure data, the term $\frac{dP}{dt}$ in equation 10 suffers from large magnitudes of interference. Due to this, a moving average filtering scheme was implemented both on the pressure trace and the heat transfer curve. It was also made sure that with this filtering scheme the shift in the pressure trace was not significant. This can be seen in Figure 23.

To obtain a better heat transfer result, equation 11 presented by Pipitone (9) was used which assigns an additional term to equation 10 to include the effect of blow-by, hence eliminating the error in the result of the heat transfer rate. The result from this equation is also shown in Figure 22.

$$-\frac{dQ}{dt} = p\frac{dV}{dt} + \frac{dU}{dt} \quad \ldots (9)$$

$$-\frac{dQ}{dt} = \frac{\gamma}{\gamma-1}.p.\frac{dV}{dt} + \frac{1}{\gamma-1}.V.\frac{dP}{dt} \quad \ldots (10)$$

$$-\frac{dQ}{dt} = \frac{\gamma}{\gamma-1}p.\frac{dV}{dt} + \frac{1}{\gamma-1}.V.\frac{dP}{dt} - \frac{\gamma}{\gamma-1}.\frac{pV}{m}.\frac{dm}{dt} \quad \ldots (11)$$

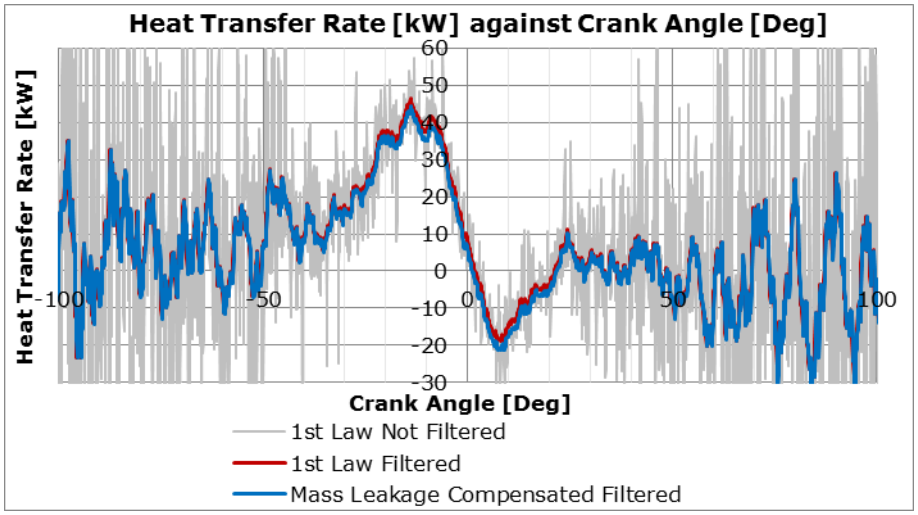

Figure 22: The graph of heat transfer rate against crank angle – 3000rpm; 84bar.

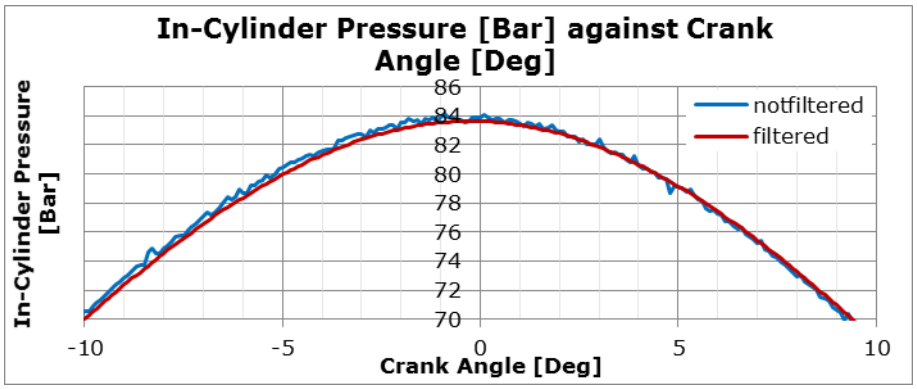

Figure 23: Comparison graph between filtered and unfiltered experimental in-cylinder pressure data – 3000rpm; 84bar.

Equations 10 and 11 shows that the ratio of specific heats is required in the calculation of heat transfer. It is known that the ratio of specific heats vary significantly with temperature, as shown in Figure 24 for the same setpoint of 3000rpm; 84bar. Equations 10 and 11 were used with a varying gamma according to Figure 24. The heat transfer obtained in Figure 22 shows a good match to work published by the previously mentioned authors; Lawton (13), Wendland (14) and Pinfold (15), where the heat transfer from the cylinder peaks at an angle of around 11DegCA before peak in-cylinder temperature and drops down to below zero shortly after TDC, when the temperature is still very close to its maximum value. On the other hand, such result is detached from that of Figure 21 which was obtained through simulation by using Annand's and Woschni's correlations, where the peak heat transfer occurs very close to TDC and no heat flow reversal was shown just after TDC. To show better the comparison between the heat transfer calculated from the first law and that obtained through Annand's and Woschni's correlations, Figure 25 was plotted.

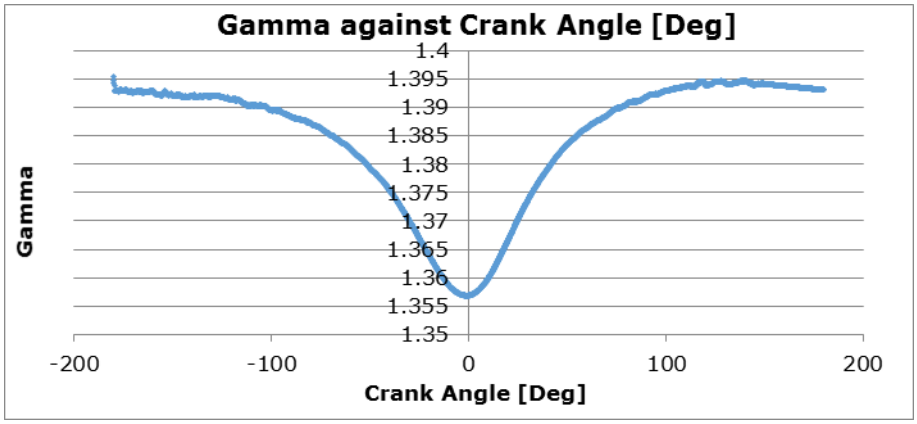

Figure 24: The graph of specific heat capacity ratio variation against crank angle.

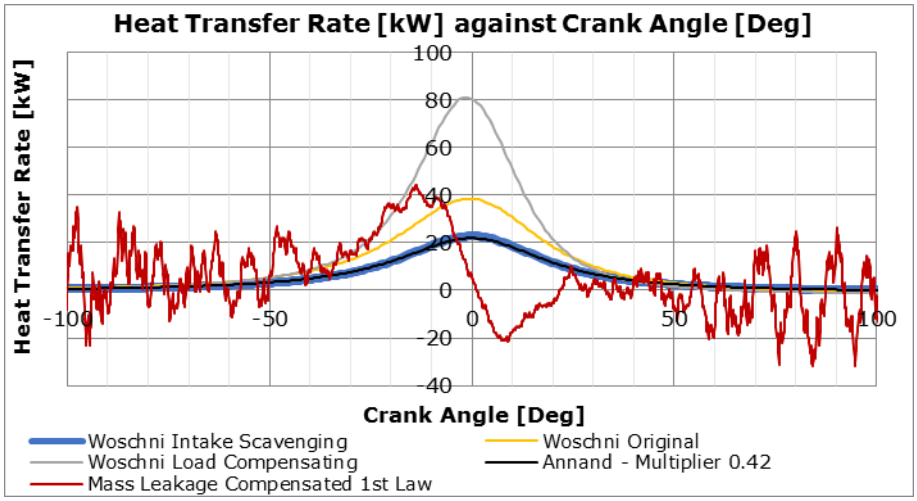

Figure 25: The graph of heat transfer rate against crank angle, comparing different models to the calculated heat transfer – 3000rpm; 84bar.

The heat transfer computation from equations 10 and 11, requires the in-cylinder volume and its rate of change. In turn, to obtain the volume from the crank-slider equation, the compression ratio is required. It had been said previously that usually the true CR for an engine varies from that quoted by the OEM due to tolerances of manufacturing, thermal expansions and cyclic loadings in the engine structure. The sensitivity of the heat transfer determined from equations 10 and 11 due to CR used in the crank-slider equation was investigated. Figure 26 was plotted for the 3000rpm; 84 bar with a CR of 17.3:1. Variations of ±5% and ±10% from 17.3:1 were intentionally imposed on the same experimental in-cylinder pressure data to obtain the resulting heat transfer rate, as given also in Figure 26. It can be seen that for 5% variation on a CR of 17.3:1, an error of around 48% in the peak heat transfer rate resulted. Also, biasing further the CR would result in the loss of the early peak heat transfer and negative heat transfer characteristic just after TDC.

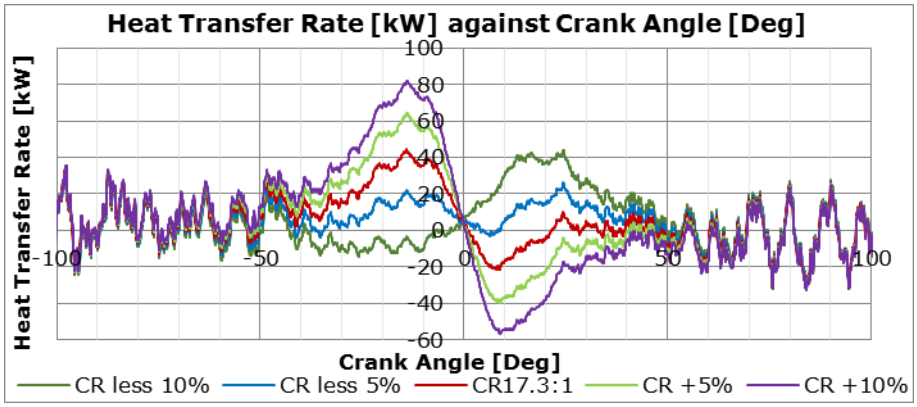

Figure 26: The graph of heat transfer rate against crank angle showing difference in heat transfer due to CR uncertainty – 3000rpm; 84bar.

Trapped Mass

On the experimental pressurized motoring setup, no measurement of gas mass flow was conducted. After calibrating the one-dimensional simulation to the experimental in-cylinder pressure data, the trapped mass was obtained as shown in Figure 27 for the case of 3000rpm; 84bar, where the cycle starts with the compression stroke, and compared to that calculated from experimental values. It should be said that in the calculation on experimental values, since the gas temperature can only be predicted during closed valves period, the gas temperature during the intake and exhaust strokes was taken to be equal to the measured shunt pipe temperature. During closed valves period, the trapped mass was calculated using the initial trapped mass estimated at IVC, and decreasing the mass flowing out as blow-by per crank angle. On the other hand, during gas exchange periods, the entrapped mass had to be calculated using the ideal gas law equation.

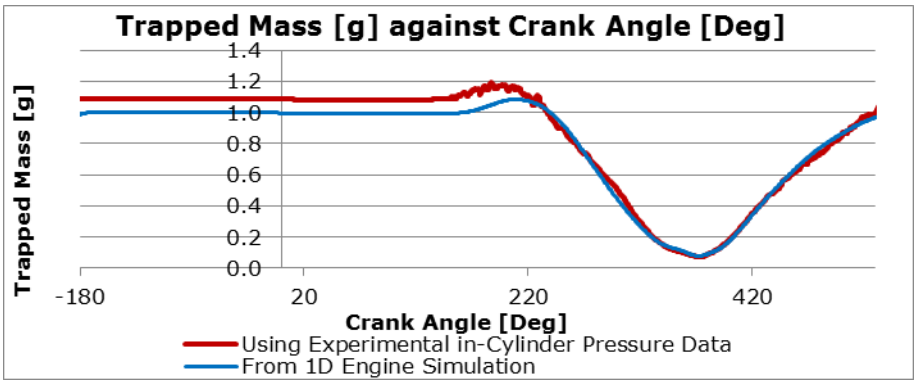

Figure 27: The graph of trapped mass against crank angle for the 3000rpm; 84bar

DISCUSSIONS AND CONCLUSIONS

As stated earlier in this publication, the main aim of this work was to use the experimental data obtained in the previous work (3) to develop and calibrate a one-dimensional model, with the hope of identifying any shortcomings in the experimental data, or simulation strategies. The results obtained confirm that the one-dimensional simulation software is able to model the pressurized motoring setup successfully when operating with air as the pressurization gas. The quantity and quality of the experimental data obtained in (1) (2) (3) seem to provide adequate information for the one-dimensional analyst to calibrate a one-dimensional model.

As discussed in the previous section of heat transfer and namely figure 25, the heat transfer models still used in one-dimensional simulation were found to deviate from the experimentally obtained heat transfer and are not able to capture the early peak in heat transfer out of the cylinder and the negative heat transfer just after TDC. It was shown that the characteristic where the heat transfer from the cylinder peaks at an angle of around 11DegCA before peak in-cylinder temperature and drops down to below zero shortly after TDC, (when the temperature is still very close to its maximum value) is in agreement with work published previously (Lawton (13), Wendland (14) and Pinfold (15)). However this characteristic is not in agreement with that obtained through simulation by using Annand‘s and Woschni‘s correlations (where the peak heat transfer occurs very close to TDC and no heat flow reversal was shown just after TDC).

The FMEP model given by Chen and Flynn (8) showed acceptable agreement with experimental data.

The relatively good agreement between one-dimensional results and those obtained experimentally also puts more confidence in the experimental data obtained from the pressurized motoring setup.

The blow-by simulation proved to be relatively straight forward and gave successful results, which agreed with that obtained experimentally. Such model resulted in a slight increase in computational time, which for large DOEs might be significant. From the simulation it was found that blow-by has a small contribution to the loss angle and peak-pressure magnitude when compared to heat loss.

The simulation generated in-cylinder pressure can be used as an intelligent filter to the experimental in-cylinder pressure, if well calibrated. It should however be noted that due to the deficiency of the heat transfer models which are imposed on the in-cylinder pressure generated from simulation, some deviations will surely be present. The simulation in-cylinder pressure generated was also found to be a relatively good pegging reference for the experimental in-cylinder pressure traces.

SUGGESTIONS FOR FURTHER WORK

Having calibrated a one-dimensional model with the experimental data obtained in previous work gave the authors the chance to experience the requirements from experimental data from the point of view of the one-dimensional analyst. This showed that the experimental data obtained was adequate; however one quantity which would have been useful had it been measured was the trapped mass, or the mass air flow into the engine. Such quantity was required when calibrating the intake stroke, but since such experimental data was not available, a simple calculation using the ideal gas law had to be done instead. Such result shows that if the mass flow into the cylinders would be measured in future experiments; a better correlated model can be achieved.

As was discussed, none of the available heat transfer models were able to capture adequately the heat transfer from the engine. Therefore a user-defined heat transfer model, which is easily implemented, could have resulted in much better results from the simulation software. If such difficulty is overcome, future work can include the development of a user-defined model based on equation 11 which would be able to give the crank-resolved heat transfer.

To obtain better confidence in the one-dimensional model, the cylinder head, piston and liner temperatures can be compared to that achieved experimentally had such values been available from experimental sessions. The pressurized motoring setup at University of Malta is being modified at the moment to include two eroding type, transient surface thermocouples which is hoped to address the heat transfer analysis experimentally.

ACKNOWLEDGEMENTS

Mr. Andrew Briffa is thanked for his assistance in setting up the flow bench used in this research.

The research work disclosed in this publication is partially funded by the Endeavour Scholarship Scheme (Malta). Scholarships are part-financed by the European Union-European Social Fund (ESF)-Operational Programme II–Cohesion Policy 2014-2020 "Investing in human capital to create more opportunities and promote the well-being of society".

REFERENCE LIST

1. Caruana C, Farrugia M, Sammut G. The Determination of Motored Engine Friction by Use of Pressurized 'Shunt' Pipe between Exhaust and Intake Manifolds. SAE Technical Paper 2018-01-0121. 2018.
2. Caruana C, Farrugia M, Sammut G, Pipitone E. Further Experimental Investigation of Motored Engine Friction Using Shunt Pipe Method. SAE Technical Paper 2019-01-0930. 2019.
3. Caruana C, Pipitone E, Farrugia M, Sammut G. Experimental investigation on the use of Argon to improve FMEP determination through motoring method. SAE Technical Paper 2019-24-0141, SAE Naples ICE2019 14th International Conference on Engines and Vehicles, Capri, Napoli. 15th - 19th September, 2019.
4. Camilleri S. Investigation of Common Rail Diesel Engine. Msida: Undergraduate Dissertation, University of Malta; 2010.
5. Caruana C, Azzopardi JP, Farrugia M, Farrugia M. Common rail diesel engine, fuel pressure

control scheme and the use of speed — Density control. In IEEE 25th Mediterranean Conference on Control and Automation (MED); 2017; Valletta, Malta. ISBN: 978-1-5090-4533-4. p. 201-216.

6. Annand WJA. Heat Transfer in the Cylinders of Reciprocating Internal Combustion Engines. Proc. Inst. Mech. Engrs. 1963; 177(1).
7. Woschni G. A Universally Applicable Equation for the Instantaneous Heat Transfer Coefficient in the Internal Combustion Engine. SAE Technical Paper 670931. 1967.
8. Ricardo. WAVE User Manual. Ricardo; 2017.
9. Pipitone E, Beccari A. Determination of TDC in internal combustion engines by a newly developed thermodynamic approach. Applied Thermal Engineering. 2010;: p. 1914 - 1926.
10. Heywood JB. Appendix C: Equations for Fluid Flow through a Restriction. In Heywood JB. Internal Combustion Engine Fundamentals.: McGraw-Hill; 1988. p. 906 - 909.
11. Farrugia M. FSAE: Engine Simulation with WAVE. Michigan: Oakland University; 2004, https://software.ricardo.com/resources/fsae-engine-simulation-with-wave.
12. Randolph A. Methods of Processing Cylinder-Pressure Transducer Signals to Maximise Data Accuracy. SAE Technical Paper, 900170. 1990.
13. Lawton B. Effect of Compression and Expansion on Instantaneous Heat Transfer in Reciprocating Internal Combustion Engines. Proc. Instn. Mech. Enginrs., Part A, Journal of Power and Energy. 1987; 201: p. 175-186.
14. Wendland DW. The Effect of Periodic Pressure and Temperature Fluctuations on Unsteady Heat Transfer in a Closed System. Wisconsin:; 1968.
15. Annand WJD, Pinfold D. Heat Transfer in the Cylinder of a Motored Reciprocating Engine. SAE Technical Paper 800457. 1980.
16. Heywood JB. Combustion in Compression Ignition Engines. In Heywood JB. Internal Combustion Engine Fundamentals.: McGraw-Hill; 1988. p. 508 - 510.